Numerical Study on the Ducted Scramjet Combustor

Sang Gon Lee* and Sang Hun Kang**[†]

* Department of Aerospace Information Engineering, Konkuk University, 05029 Seoul, South Korea,
samho2116@konkuk.ac.kr

**Department of Mechanical and Aerospace Engineering, Konkuk University, 05029 Seoul, South Korea
aeroksh@konkuk.ac.kr

[†] Corresponding Author

Abstract

To enhance the secondary combustion efficiency of the fuel-rich mixture in the ducted scramjet's gas generator, careful consideration is required for the combustor geometry design. In this study, the impact of varying flow characteristics, specifically the divergence angle, in a ducted scramjet combustor on the trajectory and combustion of solid particles is examined through numerical analysis. Results show that increased divergence angle leads to higher flow velocity, reducing particle heating residence time. Insufficient combustion time lowers particle temperature and combustion efficiency. Hence, when designing a ducted scramjet, the combustor's geometry, including the divergence angle, and ambient flow must be considered.

1. Introduction

The scramjet engine, which is one of the hypersonic air-breathing propulsion systems, is being actively researched worldwide. Most fuels utilized to generate thrust in scramjet engines are hydrocarbons, such as JP-10 and kerosene, as well as hydrogen. Gaseous and liquid fuels are predominantly employed [1-2]. Although the use of these fuels increases the complexity of the engine system, they offer advantages such as easy control of the fuel-to-air ratio and high heating value [3]. Consequently, liquid and gaseous fuels have been the primary fuels for scramjet engines, with numerous studies conducted over a long period of time [4-6]. Conversely, solid fuel-based hypersonic air-breathing propulsion systems possess advantages in terms of simplicity of structure and low maintenance costs. However, they exhibit relatively low thrust and combustion efficiency, and there is limited research in this area [7-9].

To overcome the limitations of conventional solid fuel scramjets, Zhong Lv et al. proposed a new concept known as a solid-fuel rocket scramjet [10]. This solid-fuel rocket scramjet shares a similar structure to a ducted ramjet, and hence is referred to as a "Ducted Scramjet" in this study [11]. It can be observed that a ducted scramjet resembles existing scramjets, composed of an Inlet, Isolator, Combustor, and Nozzle, which use gaseous and liquid fuels. However, in the case of a ducted scramjet, a solid fuel gas generator is introduced to combust the fuel-rich propellant. The operational sequence of the combustor in a ducted scramjet is as follows: Initially, the fuel-rich solid propellant is burned in the gas generator, and the resultant fuel-rich mixture is injected into the main combustor. This mixture, consisting of fuel-rich gas and solid particles, combines with the supersonic airflow entering through the inlet, leading to secondary combustion within the main combustor. During this process, the fuel injected from the gas generator maintains a sufficiently high temperature to support secondary combustion in the main combustor, eliminating the need for a separate igniter. Additionally, the ducted scramjet offers the advantage of flame holding and fuel-to-air ratio control.

Due to the aforementioned advantages, extensive research on ducted scramjets has been actively conducted recently. In particular, significant efforts have been made to enhance combustion efficiency [12-16]. As mentioned earlier, the fuel-rich mixture comprises fuel-rich gas and solid particles. Improving the combustion efficiency of both fuels is crucial for enhancing the performance of ducted scramjets. The residence time of solid particles within the combustor, which directly impacts their combustion efficiency, is influenced by the combustor's geometry. Therefore, the design of the combustor plays a vital role [12]. Li et al. conducted a study analyzing the combustion performance based on the shape of vortex generators and demonstrated that the combustion performance varies significantly depending on the geometry of the combustor [16].

In the design of a scramjet, the internal flow characteristics can vary significantly depending on the internal flow passage, primarily due to the presence of supersonic flow. Huang et al. conducted a study on the flow characteristics by varying the divergence angle of the scramjet isolator by 0.5 degrees, and they confirmed that even slight angle variations have a noticeable impact on the flow characteristics [17]. Considering that the trajectory of solid particles is

directly influenced by the altered internal flow, it is crucial to design the system with an appropriate divergence angle [18]. However, there is still limited research on the effect of the combustor divergence angle on combustion performance and the trajectory of solid particles in ducted scramjets. Therefore, the objective of this study is to investigate the influence of flow characteristic variations caused by the divergence angle in the ducted scramjet combustor on the trajectory and combustion characteristics of solid particles through numerical analysis.
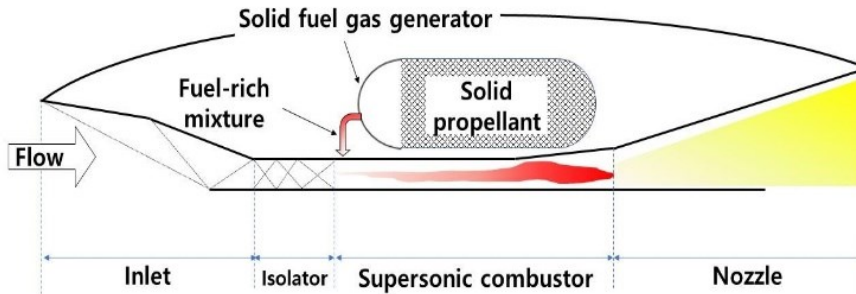

Figure 1: Schematic of ducted scramjet

2. Geometry and numerical method

2.1 Combustor geometry and grid details

In this study, we utilized the combustor model proposed by Li et al. [12] and examined the trajectory and combustion performance of solid particles by varying the divergence angle by ±1° to investigate the flow characteristics. Figure 2 illustrates the baseline three-dimensional model employed in this study. The overall length of the combustor model, including the isolator and supersonic combustor, is 1 300mm, with the isolator having an expansion angle of 1°. The supersonic combustor is connected to the isolator, and fuel, comprising carbon particles and unburned gas generated from the solid fuel gas generator, is injected from the upper wall. The fuel injector is a single 13.5mm-diameter wall jet injector positioned at an injection angle of 60°. To prevent the backflow of high-pressure combustion gas and avoid unstart, a 15mm backward-facing step is incorporated in front of the injector. The baseline model has a combustor divergence angle of approximately 2.37°. Additionally, to assess the impact of varying the divergence angle, we modified the combustor divergence angle of the baseline model by ±1°, as depicted in Figure 3.

Table 1 displays the combustor divergence angle and the number of grid cells for each case. The grid system is generated as a three-dimensional structured grid, with the y^+ value set to less than 1 for supersonic flow analysis on the wall. Figure 4 illustrates the grid system for the baseline model.
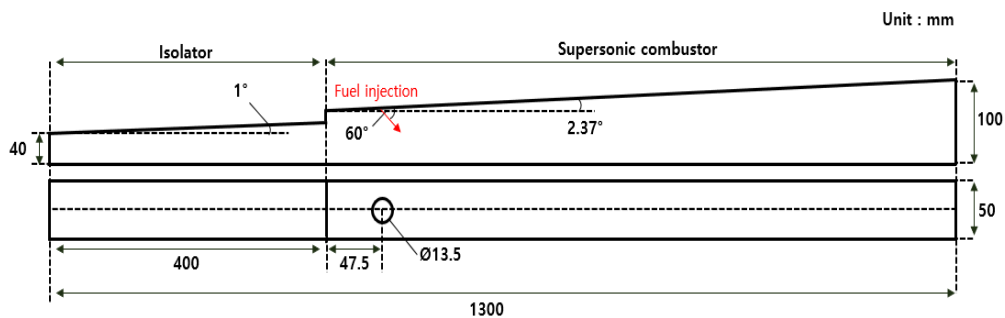

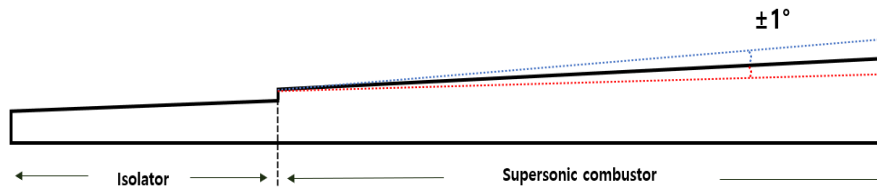Figure 2: Schematic of the baseline model

Figure 3: Schematic according to combustor divergence angle

Table 1: Combustor divergence angle and number of grid cells for case

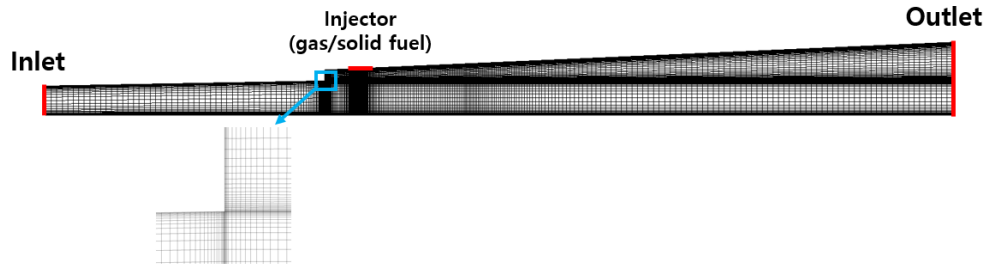|	**Combustor divergence angle**	**Grid(cell)**
Case1	1.37°	1.7million
Case2 (Baseline model)	2.37°	1.8million
Case3	3.37°	2.0million

Figure 4: Grid system of the baseline model

2.2 Numerical method and boundary condition

To investigate the influence of changes in flow patterns resulting from variations in the divergence angle on the trajectory and combustion of solid particles, numerical analysis is performed using the commercial software ANSYS FLUENT. As mentioned earlier, since the fuel injected from the gas generator comprises both gas and solid particles, it is essential to employ multiphase flow analysis that considers the gas/solid phases.

In the gas phase, a three-dimensional RANS (Reynolds Averaged Navier-Stokes equations) steady-state analysis is performed using a density-based solver. Turbulence effects are accounted for using the k-omega SST model. The flux scheme utilizes the Roe-FDS (Roe flux-difference splitting) scheme.

In the solid phase, the Discrete Phase Model (DPM) utilizing the Euler-Lagrange approach is employed to analyze the trajectory and combustion performance of solid particles. This approach allows for the analysis of particle behavior using the Lagrangian method within a flow field analyzed using the Eulerian method. To employ the DPM, it is generally recommended to have a low volume fraction of particles, typically around 10-12% of the total volume. In this model's combustor, the volume fraction of particles is sufficiently low, less than 1%, making the DPM a suitable method to employ. For computational simplicity, only carbon particles are considered. Furthermore, the Discrete Random Walk Model is applied to account for particle diffusion caused by turbulence.

Tables 2 and 3 present the boundary conditions and the composition of the fuel-rich gas injected from the gas generator for numerical analysis. The design condition corresponds to an altitude of 25 km and a Mach number of 6, therefore, the Mach number at the inlet of the combustor model is set to 2. The walls are set as no-slip, adiabatic walls.

Table 2: Boundary condition

Boundary		Total Pressure [kPa]	Static Pressure [kPa]	Total Temperature [K]	Etc.
Inlet		1 190	152	1 818	
Outlet			100	300	
Injector	Gas phase	700	370	1 460	
	Solid phase				Mass Flow Rate 0.03 kg/s
Wall					No-slip, adiabatic

Table 3: Fuel injection condition

	Gas-Phase[%]			Solid-Phase[%]	
CO	49.2	HCl	22.7	C	65.2
H_2	14.2	N_2	11.6	Al_2O_3	19.2
CH_4	1.7	H_2O	0.5	MgO	15.6

2.3 Combustion model

The combustion model is configured to account for the reaction of multi-phase flow. In the gas phase, turbulence plays a significant role in combustion within supersonic flow. Therefore, the combustion model employs the finite-rate/eddy-dissipation model, which considers both the chemical reaction rate and turbulence intensity. Among the 6 species ($CO, H_2, CH_4, HCl, N_2, H_2O$) injected from the fuel injection, chemistry models are set up for the combustible species (CO, H_2, CH_4). To reduce computation time, a single-step reaction is utilized. Table 4 presents the three single-step reaction mechanisms employed in this study [19]. The reaction rate coefficient can be determined using Eq. (1).

Table 4: Reaction and rate coefficient

Reaction	Pre-exponential factor, A	Activation energy, E_A
$2CO + O_2 \rightarrow 2CO_2$	2.239×10^{12}	1.7×10^8
$2H_2 + O_2 \rightarrow 2H_2O$	9.87×10^8	3.1×10^7
$CH_4 + 2O_2 \rightarrow CO_2 + 2H_2O$	2.119×10^{11}	2.027×10^8

$$k(T) = Aexp(-\frac{E_A}{R_u T}) \tag{1}$$

To account for the surface diffusion rate and chemical reaction rate of solid particles, the combustion model utilizes the kinetic/diffusion-limited model proposed by Baum and Street [20]. The reaction of carbon particles is represented as $C<s> + O_2 \rightarrow CO_2$, and the diffusion rate coefficient and particle reaction rate coefficient can be determined using Eq. (2) and (3). Here, C_1 represents the constant, T_p is the particle temperature, and d_p is the particle diameter. Wang conducted experiments confirming that the diameter of solid particles generated from the gas generator ranges from 0.5 to 80 μm [14]. For simplicity in this study, the size of solid particles is uniformly set to 10 μm [14].

$$D_0 = C_1 \frac{\left[\frac{T_p + T}{2}\right]^{0.75}}{d_p} \tag{2}$$

$$k_p(T) = Aexp(-\frac{E_A}{R_u T_p}) \tag{3}$$

3. Results and discussion

3.1 Analysis of effects of divergence angle on the flow characteristics

By employing the aforementioned numerical methods, the combustion phenomena of the three combustor models are analyzed. Figure 5 illustrates the Mach number and pressure contours across the entire combustor region. In all cases, a Mach 2 flow enters the combustor inlet through the isolator, where it mixes with the fuel injected at the upper wall, resulting in combustion. Due to the mixing and combustion of air and fuel, the flow velocity decreases while the pressure increases. However, as the divergence angle increases, the Mach number also increases, leading to a tendency for the high-pressure area to decrease throughout the overall combustor.
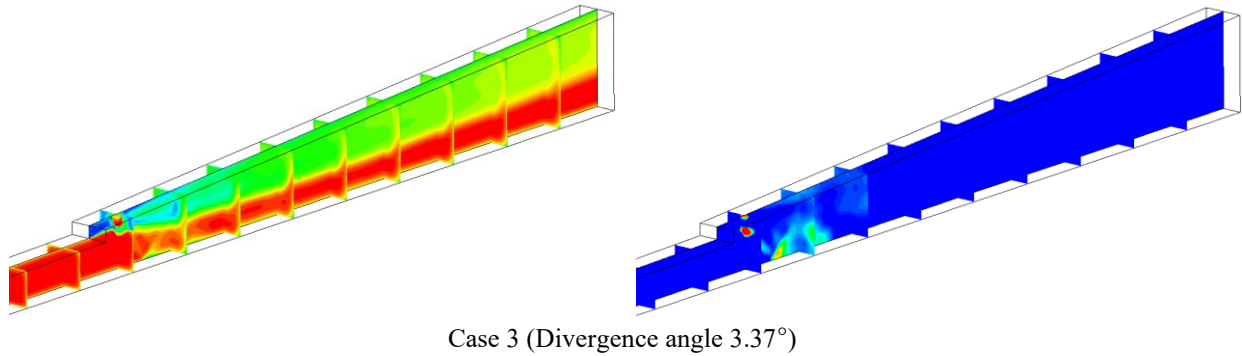

Case 1 (Divergence angle 1.37°)

Case 2 (Divergence angle 2.37°)

Case 3 (Divergence angle 3.37°)
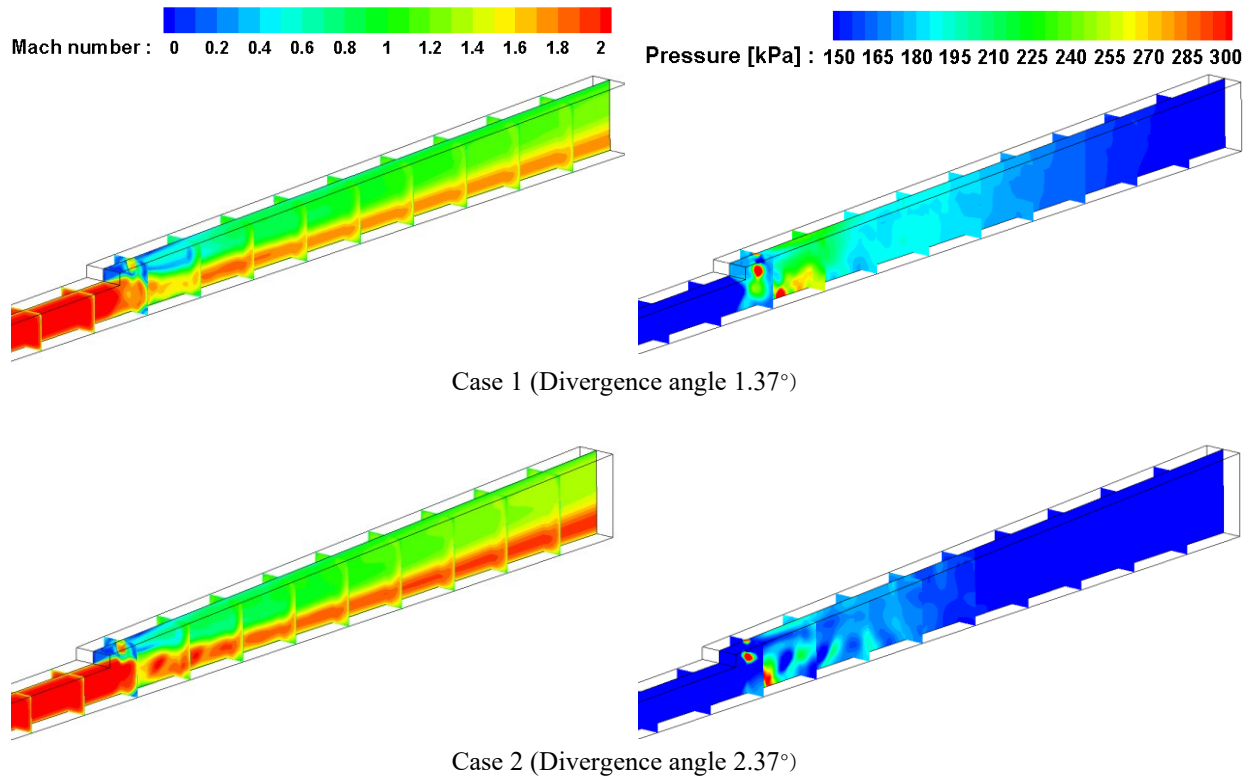
Figure 5: Mach number contours**(left)** and Pressure contours**(right)**

To provide a more detailed understanding of the Mach number and pressure variations with respect to the divergence angle, the Mach number and pressure within the region where fuel is injected and mixed (x=0.36 to 0.62 m) are compared in Figure 6. The figure shows complex interactions occurring when the fuel injected from the upper wall at sonic speed is mixed with the incoming supersonic air flow. In the injector area, a bow shock is generated by the jet, and the shock wave is reflected by the bottom wall, resulting in a reflected shock. However, in the region between the entrance of the combustor and the jet, it can be observed that the shock wave is generated further upstream as the divergence angle decreases. Downstream of the injector, where combustion is expected to occur as a result of fuel and air mixing, the pressure increases due to combustion. However, the magnitude of pressure increase varies for each case. Specifically, the pressure increases more significantly when the divergence angle is smaller, resulting in a corresponding larger decrease in the Mach number.
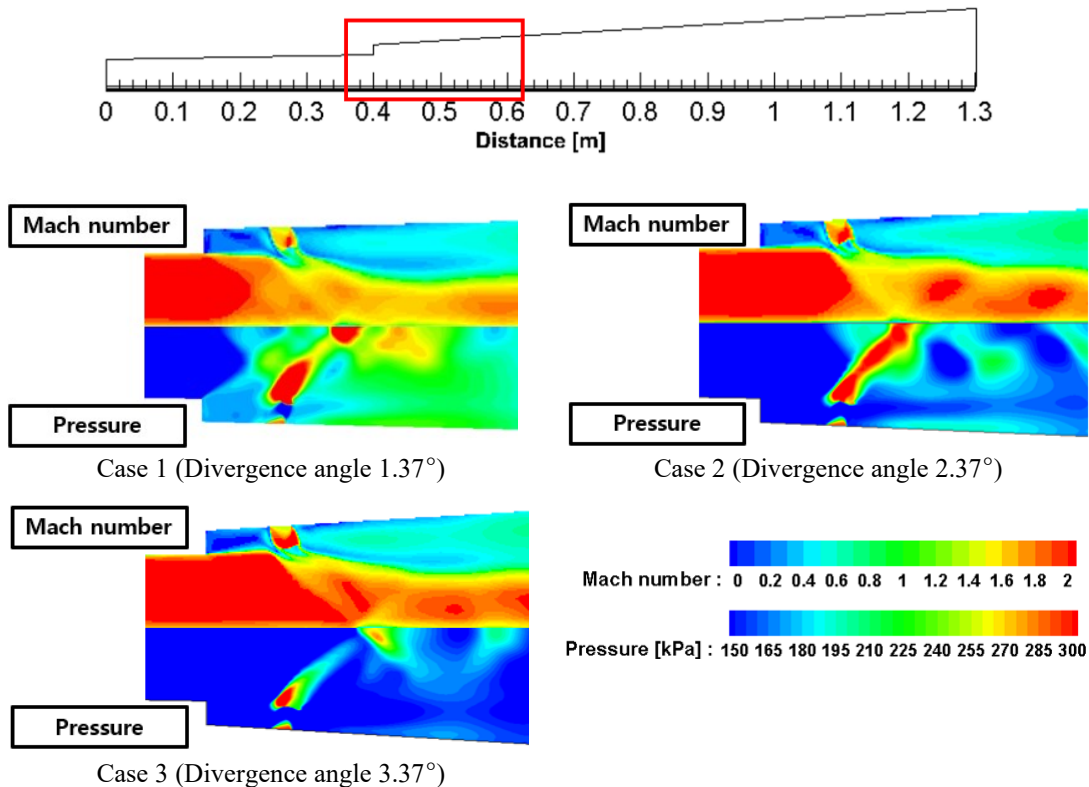

Case 1 (Divergence angle 1.37°)

Case 2 (Divergence angle 2.37°)

Case 3 (Divergence angle 3.37°)

Figure 6: Comparison of flow characteristics in the injector region(symmetric plane)

To confirm the decrease in Mach number and increase in pressure due to the combustion, the static temperature and the H_2O mass fraction contour are presented in Figure 7. In Case 1 and 2, a distinct high-temperature region exceeding 3 000 K is observed in the central region of the combustor. Additionally, the combustion product, represented by the H_2O mass fraction, is prominently generated in the middle of the combustor; however, diminishes downstream. In

Case 3, a clear high-temperature region exceeding 3 000 K is not observed, but combustion occurs uniformly throughout all areas. This can be attributed to the augmented expansion effect of the flow with higher divergence angles, resulting in increased Mach numbers. Consequently, the residence time of the fuel in the combustor decreases, leading to more active combustion downstream.
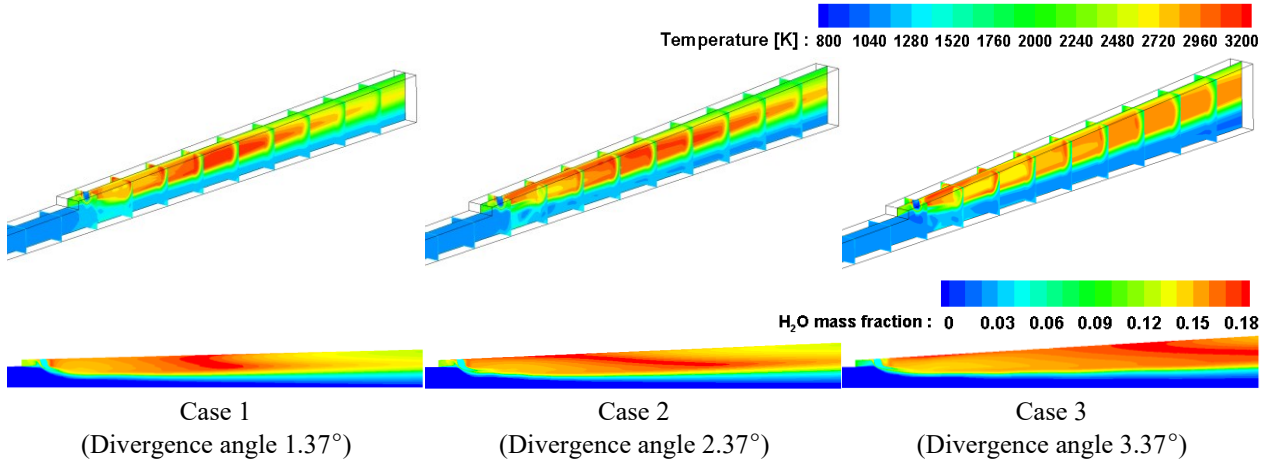

Temperature [K] : 800 1040 1280 1520 1760 2000 2240 2480 2720 2960 3200

H_2O mass fraction : 0 0.03 0.06 0.09 0.12 0.15 0.18

| Case 1 | Case 2 | Case 3 |
| (Divergence angle 1.37°) | (Divergence angle 2.37°) | (Divergence angle 3.37°) |

Figure 7: Static temperature contours **(up)**
and H_2O mass fraction contours at the symmetry plane **(down)**

To quantitatively analyze the flow characteristics within the combustor model, area-weighted average Mach numbers and pressures are presented in Figure 8. As depicted in the figure, the pressure experiences a sharp increase near the fuel injector and then gradually decreases around x=0.6 m. This phenomenon can be attributed to the mixing and combustion of the injected fuel and air, leading to a rise in pressure. However, as the flow expands in the diverging combustor, the pressure gradually decreases. The Mach number distribution reveals that the incoming flow, initially at Mach number 2, undergoes rapid deceleration in the vicinity of the injector region due to combustion. However, beyond this point, the flow accelerates from approximately x=0.6 m as a result of the supersonic flow expansion in the diverging combustor. Notably, as the divergence angle increases, the expansion and acceleration of the flow become more pronounced, resulting in higher velocity and lower pressure.
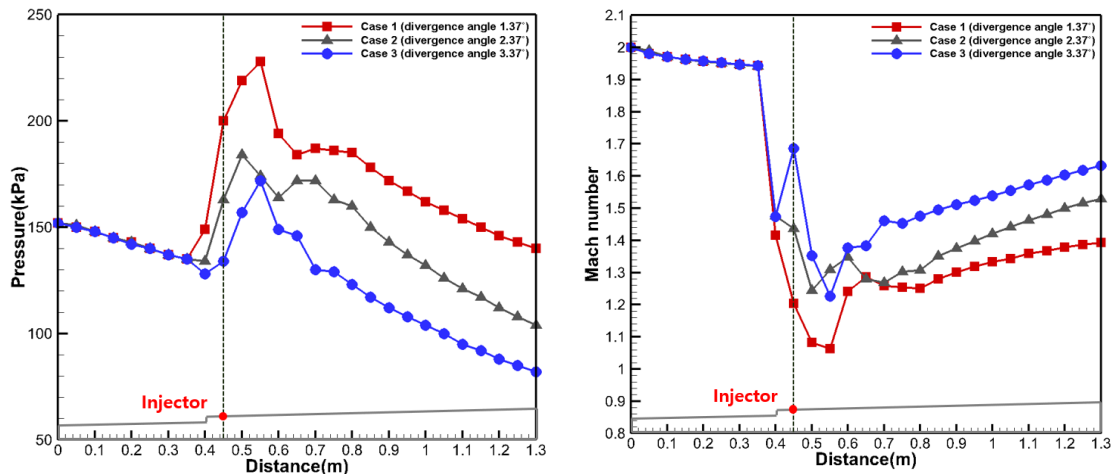

Figure 8: Area weighted average pressure **(left)** and Mach number **(right)** distributions

3.2 Carbon particle combustion analysis

As mentioned previously, the expansion and acceleration of the flow become more prominent with increasing divergence angle. Consequently, the residence time of the fuel decreases, leading to less active combustion. To evaluate the influence of flow characteristics on the behavior of carbon particles, Figure 9 presents the properties of the particles, including velocity, residence time, temperature, and mass distribution. As depicted in the figure, case 3 exhibits the

highest particle velocity and the shortest residence time. This can be attributed to the increased flow velocity resulting from the larger divergence angle. Conversely, when comparing the maximum particle temperature within the combustor, case 1 shows the highest temperature. This is due to the lower particle velocity and the presence of a high-temperature gas phase region located upstream (refer to Figure 7), allowing sufficient time for the particle temperature to rise. Regarding the particle mass distribution, case 1 displays the most significant decrease in mass, indicating active surface combustion. However, in case 3, the high particle velocity and the absence of a high-temperature gas phase region exceeding 3,000 K limit the rise in particle temperature. This indicates that surface combustion is not as active, resulting in a smaller reduction in particle mass in case 3.

To provide a clearer view of the changes in particle residence time and temperature, Figure 10 illustrates the maximum particle temperature and longest residence time values within the combustor for each case. It can be observed that as the divergence angle decreases, both the maximum particle temperature and longest residence time values decrease. Specifically, the maximum particle temperature between case 1 and case 3 shows a difference of 15%, while the longest residence time differs by up to 12%.

The divergence angle directly influences the residence time and temperature of particles, which are closely associated with fuel combustion efficiency. To evaluate the impact of divergence angle on combustion efficiency, the carbon particle combustion efficiency is computed using Eq. (4) and depicted in Figure 11. Here, $m_{c-fule\ inlet}$ represents the total mass of carbon particles injected from the injector, while m_{C-exit} denotes the total mass of carbon particles exiting the combustor. As depicted in the figure, case 1 exhibits the highest combustion efficiency among the three cases, with a value that is 10% greater than that of case 3.

$$\eta_{particle} = \left(1 - \frac{m_{C-exit}}{m_{c-fule\ inlet}}\right) \times 100 \ [\%] \tag{4}$$

Case 1(Divergence angle 1.37°)   Case 2(Divergence angle 2.37°)

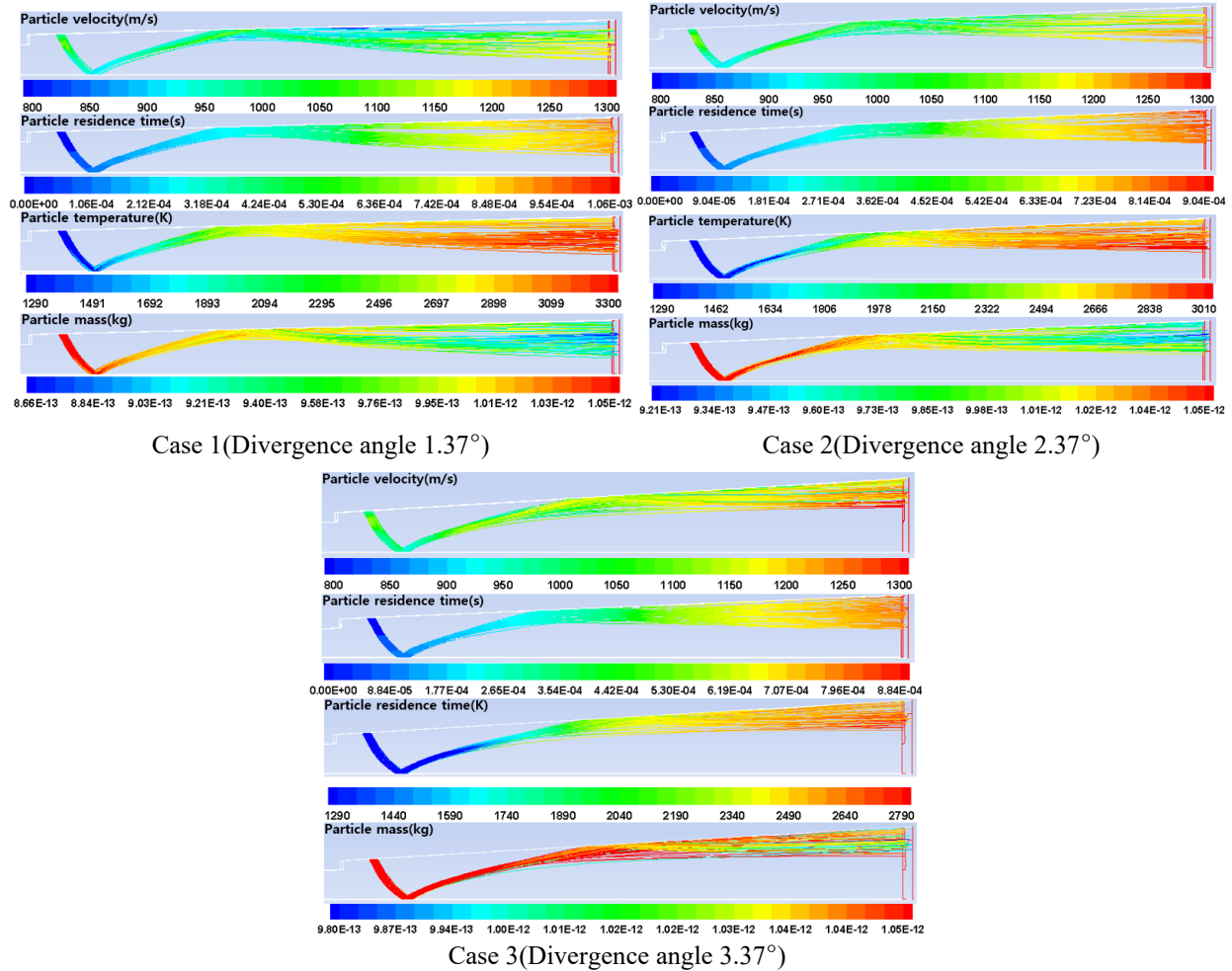Case 3(Divergence angle 3.37°)

Figure 9: Carbon particle contours
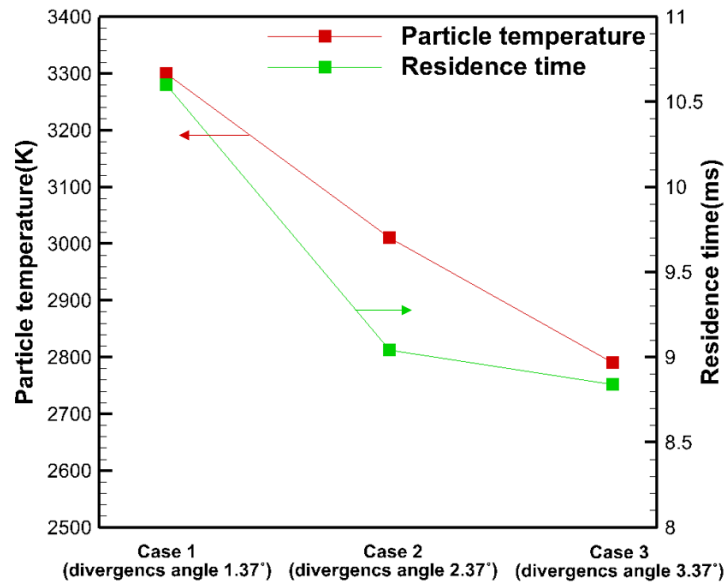(Particle velocity, residence time, temperature, mass)

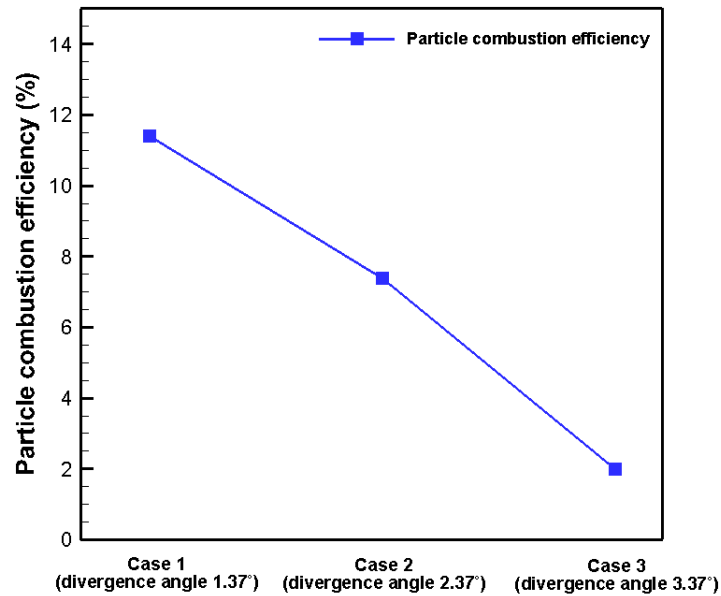Figure 10: Max. particle temperature and longest residence time

Figure 11: Carbon combustion efficiency

4. Conclusions

The impact of flow characteristics, which vary with the divergence angle of the ducted scramjet combustor, on the trajectory and combustion characteristics of solid particles was investigated through numerical analysis. The findings from the numerical analysis are as follows:

1. The analysis of flow characteristics revealed that an increase in the divergence angle led to an increase in flow velocity and a decrease in pressure.
2. The variation in flow characteristics had a notable effect on the trajectory and characteristics of carbon particles. The increased divergence angle resulted in higher particle velocities, shorter residence times, and lower particle temperatures.

3. Due to the reduced residence time for particle heating, there was insufficient time for combustion to occur, leading to decreased particle surface combustion and limited reduction in particle mass.

4. The changes in flow characteristics and combustion behavior resulted in significant variations in combustion efficiency, with differences of up to 10% observed with different divergence angles.

These findings highlight the significant influence of combustor geometry and supersonic flow on the secondary combustion of fuel in a ducted scramjet. Therefore, when designing a ducted scramjet, it is crucial to consider the geometry of the combustor, as well as the ambient flow of particles, including the divergence angle.

References

[1] Alff, F., Brummund, U., Clauss, W., Oschwald, M., Sender, J., and Waidmann, W. 1994. Experimental Investigation of the Combustion Process in a Supersonic Combustion Ramjet (SCRAMJET) Combustion Chamber. DGLR-Jahrestagung:629-638.

[2] Yan, M., Tian, Y., and Li, L. 2023. Experimental study on the combustion process of a kerosene-fueled scramjet with strut injection. Aerosp Sci Technol 137: 1-11.

[3] Altarazi, Y. S. M., Saadon, S., Yu, J., Gires, E., Ghafir, M. F. A., and Lucas, J. 2020. On-design operation and performance characteristic of custom engine. J. Adv. Res. Fluid Mech. Therm. Sci. 70(1):144-154.

[4] Gerlinger, P., and Simsont, Y. H. 2019. Numerical investigation of scramjet strut injector cooling for different fuel mass fluxes and strut material properties at mach 8 flight conditions. Acta Astronaut. 160:353-364.

[5] Aravind, S., and Kumar, R. 2019. Supersonic combustion of hydrogen using an improved strut injection scheme. Int. J. Hydrog. 44(2):6257-6270.

[6] Gruenig, C., and Mayinger, F. 1999. Supersonic combustion of kerosene/H2-mixtures in a model scramjet combustor., Combust. Sci. and Tech. 146(1-6):1-22.

[7] Vaught, C., Witt, M., Netzer, D., and Gany, A. 1992. Investigation of solid-fuel, dual-mode combustion ramjets. J. Propuls. Power. 8(5):1004-1011.

[8] Gany, A., and Netzer, D. W. 1985. Fuel performance evaluation for the solid-fueled ramjet. Int J Turbo Jet Engines. 2(2):157–168.

[9] Ben-Arosh, R., Natan, B., Spiegler, E., and Gany, A. 1998. Fuel-air mixing in solid fuel scramjet combustors. Int J Turbo Jet Engines. 15(3):223–234.

[10] Lv, Z., Xia, Z. X., Liu, B., and Liu, Y. C. 2016. Experimental and numerical investigation of a solid-fuel rocket scramjet combustor. J. of Propulsion and Power. 32(2):273-278.

[11] Kothari, V., Mehta, Y., Shrivastav, D., and Panchal, K. 2022. Enhancement in the lift force of the Solid Fuel Ducted Ramjet (SFDR) with an increase in the controlling surface. Materials Today: Proceedings. 50:1878-1882.

[12] Li, C., Xia, Z., Ma, L., Zhao, X., and Chen, B. 2019. Numerical study on the solid fuel rocket scramjet combustor with cavity. J. of Propulsion and Power. 12(7):1-17.

[13] Xiang, Z. H. A. O., Zhixun, X. I. A., Likun, M. A., Chaolong, L. I., Chuanbo, F. A. N. G., Natan, B., and Alon, G. A. N. Y. 2022. Research progress on solid-fueled Scramjet. Chinese J. Aeronaut. 35(1):398-415.

[14] Li, C., Xia, Z., Ma, L., Zhao, X., and Chen, B. 2019. Experimental and numerical study of solid rocket scramjet combustor equipped with combined cavity and strut device. Acta Astronaut. 162:145-154.

[15] Liu, J., Wang, N. F., Wang, J., and Li, Z. Y. 2020. Optimizing combustion performance in a solid rocket scramjet engine. Aerosp Sci Technol. 99:1-8.

[16] Li, C., Zhao, X., Xia, Z., Ma, L., and Chen, B. 2019. Influence of the vortex generator on the performance of solid rocket scramjet combustor. Acta Astronaut. 164:174-183.

[17] Huang, W., Wang, Z. G., Pourkashanian, M., Ma, L., Ingham, D. B., Luo, S. B., ... and Liu, J. 2011. Numerical investigation on the shock wave transition in a three-dimensional scramjet isolator. Acta Astronaut. 68(11–12):1669–1675.

[18] Huang, H., Feng, Z., Ma, L., Yang, T., and Li, C. 2022. Numerical research on the performance of solid fuel rocket scramjet combustor. J Aerosp Eng. 236(7):1450-1461.

[19] Szubel, M., Adamczyk, W., Basista, G., and Filipowicz, M. 2017. Homogenous and heterogeneous combustion in the secondary chamber of a straw-fired batch boiler. In EPJ Web of Conferences. 143:1-11.

[20] Baum, M. M., and Street, P. J. 1971. Predicting the combustion behaviour of coal particles. Combust Sci Technol. 3(5):231-243.